Results in Physics 7 (2017) 1396–1411

Contents lists available at ScienceDirect

Results in Physics

journal homepage: www.journals.elsevier.com/results-in-physics

Comprehensive thermal and structural characterization of antimony-phosphate glass

S.Y. Moustafa, M.R. Sahar *, S.K. Ghoshal

Advanced Optical Materials Research Group, Department of Physics, Faculty of Science, Universiti Teknologi Malaysia, 81310 UTM Johor Bahru, Johor Darul Ta'azim, Malaysia

ARTICLE INFO

Article history:
Received 2 March 2017
Received in revised form 5 April 2017
Accepted 6 April 2017
Available online 11 April 2017

Keywords:
Antimony-phosphate glass
Thermal properties
Solidus temperature
Liquidus temperature
Crystalline phases

ABSTRACT

For the first time, we prepare new ternary glass systems of composition (95-x)Sb_2O_3-xP_2O_5-5MgO, where x = 45, 40, 35 mol%; (85-x)Sb_2O_3-xP_2O_5-15MgO, where x = 55, 35, 25 mol%; (75-x)Sb_2O_3-xP_2O_5-25MgO, where x = 45, 35, 25 mol%; and 60Sb_2O_3-(40-x)P_2O_5-xMgO, where x = 10, 20 mol% via melt-quenching method. Synthesized glasses are characterized using XRD, FESEM, EDX, and TG/DTA measurements. The influence of varying modifier concentrations on their thermal properties is evaluated. The XRD patterns confirmed the amorphous nature of samples. SEM images demonstrated interesting phase formation with ribbons-like texture. Five crystalline phases are evidenced in the ternary diagram which are antimony phosphate and antimony orthophosphate as major phases as well as magnesium phosphate, magnesium cyclo-tetraphosphate and cervantite as minor phases. EDX spectra detected the right elemental traces. Detailed thermal analysis of these glasses revealed their high-molecular polymer character for Sb_2O_3 content greater than 50 mol%. Three different glass transition temperatures are achieved around 276, 380–381 and 422–470 °C depending on the composition. Furthermore, the solidus and liquidus temperature are found to decrease with increasing Sb_2O_3 and increases for MgO contents till 15 mol% and then decrease, where the lowest recorded solidus temperature is 426 °C. This observation may open up new research avenues for antimony based ternary glasses and an exploitation of the derived results for optoelectronics applications, photonic devices and non-linear optical devices.

Introduction

Lately, there is an upsurge in binary and ternary glass research due to their extreme stability, economy, and easy fabrication beneficial for advanced photonic applications. Thus, constant efforts are made to get newer glass composition with modified structural, physical, thermal, and optical properties. Glass plays many varied roles in rare-earth laser systems, because glass can be made with uniformly distributed rare-earth concentrations and has great potential as a laser host medium. In addition, rare-earth doped fibers have received growing attention recently. They could have many uses as amplifiers in optical communication systems and as optical sources. Glass waveguide lasers are another interesting subject for the development of compact laser sources and amplifier devices [1,2]. Glass as host in the practical lasers is subjected to extreme operating environment so they should own optimal thermal, optical and mechanical properties, in order to withstand it. The ideal features which make the material is eligible as a host are simple to synthesis, high chemical durability and hardness, acceptable physical properties, higher absorption cross section, and higher quantum efficiency [9]. Contemporary glass scientific research focuses on the development of specialized or unusual glasses as a novel media for photonic, plasmonic and nanophotonic technologies by incorporating luminescent rare-earth ions, metal nanoparticles, semiconductor nanoparticles, etc and their hybrids [1,3,4]. Research in these fields are fast and lead to emerging areas require development of new glass compositions in this context, unlike the traditional silicate, borate and phosphate glasses, heavy metal oxide glasses like bismuth, tellurite, lead, and/or antimony acting as glass structure network formers is expected to play an active role as they possess some exciting properties like high refractive index, large transmission window, large non-linear optical properties, low phonon energy (resonance vibration of the matrix) and high dielectric constant. There has been considerable investigation on Bi-, Te- and Pb- glasses but Sb-based glasses remain vastly unexploited [5] due to their mild toxicity and complex phase formation attributes related to super-cooling. Consequently, the difficulty associated to achieving highly transparent and thermally stable antimony glasses posed new challenge. One of the most striking features of antimony trioxide or antimony

* Corresponding author.
E-mail addresses: Seham_yns@yahoo.com (S.Y. Moustafa), rahimsahar@utm.my (M.R. Sahar), sibkrishna@utm.my (S.K. Ghoshal).

http://dx.doi.org/10.1016/j.rinp.2017.04.006
2211-3797/

orthophosphates ($SbPO_4$) is associated to the existence of lone electronic pairs in one of the polyhedra corners. Consequently, it offers an opportunity to acquire different phase formations with unusual electrical and optical properties [6].

In the past, antimony glass systems are combined with others components such as halides [7,8], sulfides [9,10], heavy metal oxides [11] and alkali oxides metals glasses in the form of binary (Sb_2O_3-A_2O) and ternary (Sb_2O_3-A_2O-MmOn) with A = Li, Na, K, or Cs and M = Pb or Al [12–15] mixtures. However, literatures do not hint about the synthesis and characterizations of Sb_2O_3-P_2O_5-MgO glass systems despite their innumerable technological implications. The structures of (13.86-x)ZnO-57.93Sb_2O_3-28.21P_2O_5-xNa_2O (x = 0–12 wt.%) glasses are investigated, where $SbPO_4$ is existed mainly in the crystalline phase. The glass transition temperature is decreased from 398 to 328 °C as the Na2O concentration is increased [16]. Zinc-boro-phosphate glass system of composition 50ZnO-10B_2O_3-40P_2O_5-xSb_2O_3 (x = 0–70 mol%) is prepared to determine the effects of increasing Sb_2O_3 contents on overall properties [17]. It is demonstrated that with increasing Sb_2O_3 contents the glass transition temperature is decreased from 492 to 394 °C, and density increased from 3.12 to 4.35 g·cm^{-3} together with the molar volume from 33.5 to 41.7 cm^3·mol^{-1}. The dissolution rate at 15 mol% of Sb_2O_3 is increased from 21.2 × 106 to 34.7 × 106 g cm^{-2} min^{-1} and then decreased to 12.8 × 106 g cm^{-2}·min^{-1} at 70 mol%. Furthermore, the depolymerisation of the phosphate chains is increased with the separation of antimonate (SbO_3) structural units [17].

Another glass system based on transition metal oxides of the form 50V_2O_5-(50-x)P_2O_5-xSb_2O_3 (x = 15, 25, 35 and 40 mol%) are prepared to examine the influence of increasing Sb_2O_3 concentration on the structural and thermal properties. Homogenous amorphous phase is achieved, where the glass transition temperature first decreased from 365 to 325 °C and then increased to 330 °C at 40 mol% of Sb_2O_3. Both the glass density and molar volume is increased from 3.3 to 4.5 g. cm^{-3} and 55.8 to 64.6 cm^3·mol^{-1}, respectively. Besides, the stability is against moisture attack is remarkably improved [18]. The effect of increasing Sb_2O_3 on zinc-phosphate glasses of composition (60-x) ZnO-xSb_2O_3-40P_2O_5 (x = 0–50 mol%) is examined. The participation of Sb_2O_3 in the network is revealed by the presence of P–O–Sb linkages, where the glass transition temperature (422–377 °C), $\Delta T = T_c - T_g$ (132–78 °C) and liquidus temperature (1050–930 °C) are decreased. Moreover, the glass density (3.34–4.17 g·cm^{-3}), and molar volume (31.9–50.5 cm^3·mol^{-1}) are increased. At different Sb_2O_3 concentrations various crystallization peaks are evidenced together with high durability against moisture attack [19].

The structural evaluation of PbO-P_2O_5-Sb_2O_3 glass system is made [20], where the incorporation of Sb_2O_3 is found to generate two structural units as P–O–Sb linkage, one with high Sb^{3+} cation belong to $SbPO_4$ phase and the other with high Sb^{5+} cation belong to $SbOPO_4$ phase. The glass transition temperature exhibited broad endothermic peak in the range of 352–377 °C accompanied by a slight shift towards higher temperature. This observation is attributed to the occurrence of dissimilar structural units with diverse relaxation temperature. Increase in the crystallization temperature, thermal stability, and optical band gap is evidenced with the increase of Sb_2O_3 contents [20].

Categorically, MgO-P_2O_5 glass systems are interesting due to their peculiar structure and phase formation [21,22]. These binary oxide systems are mainly composed of four intermediate phases including magnesium ortho-phosphate ($Mg_3P_2O_8$), magnesium pyro-phosphate ($Mg_2P_2O_7$), magnesium tetra-meta-phosphate (MgP_2O_6), and magnesium ultra-phosphate (MgP_4O_{11}). In addition, MgO and O′-P_2O_5 (stable orthorhombic polymorph of P_2O_5) are also manifested in the phase diagram, which remains insoluble in the solid state at high concentration of MgO and P_2O_5, respectively [23–34]. In terms of phase transition and melting point, these compounds ($Mg_3P_2O_8$) melts at 1357 °C and encounters a polymorphic transition at 1055 °C from β-$Mg_3P_2O_8$ to α-$Mg_3P_2O_8$ [24,28]. Meanwhile, $Mg_2P_2O_7$ melts at 1385 °C and encounters two polymorphic transitions one at 68 °C and another at 1100 °C [28]. The MgP_2O_6 phase melts at 1165 °C [31] and MgP_4O_{11} melts at 910 °C. The eutectic reaction between $Mg(PO_3)_2$ and MgP_4O_{11} occurs at 772 °C [32]. The O′-P_2O_5 phase melts at 580 °C with a eutectic reaction between MgP_4O_{11} and O′-P_2O_5 at 328 °C [23,34]. Despite much effort on the synthesis and characterization of several binary and ternary glasses the magnesium-antimony-phosphate glass systems are far from being studied.

Some reports revealed the preparation of binary glass from MgO-P_2O_5 system, where the MgO, P_2O_5, MgP_2O_6, and $Mg_2P_2O_7$ phases are found to dominate within the glasses formation ranges $0.4 \leq x \leq 0.8$ mol% for P_2O_5. Much structural changes are observed under heating due to the density variation in the P-O-Mg crosslink through the glass formation or crystallization. These glass systems displayed several endothermic and exothermic reaction corresponding to the peritectic reaction (MgO + melt), liquidus phase formation, eutectic reaction or crystallization of MgP_2O_6 [35]. Yet, no studies exist on phase formation of binary oxide system of MgO-Sb_2O_3. Literature revealed the study on tetragonal crystal structure of magnesium-antimonite ($MgSb_2O_4$) [36], which are prepared using solid state reaction of MgO with Sb_2O_3 at 1100 °C in the inert atmosphere. Moreover, this system showed several

Table 1
Code and nominal composition of synthesized glass samples.

Glass codes		Composition (mol%)		
		Sb_2O_3	P_2O_5	MgO
SPM1	Series I	50	45	5
SPM2		55	40	5
SPM3		60	35	5
SPM4	Series II	30	55	15
SPM5		50	35	15
SPM6		60	25	15
SPM7	Series III	30	45	25
SPM8		40	35	25
SPM9		50	25	25
SPM10	Series IV	60	30	10
SPM11		60	20	20

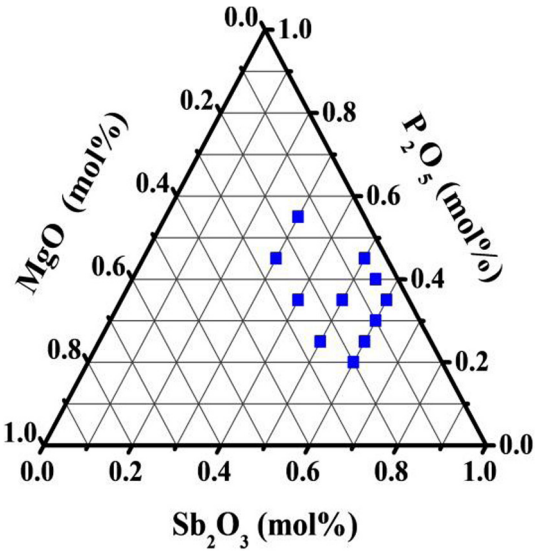

Fig. 1. Glass formation region.

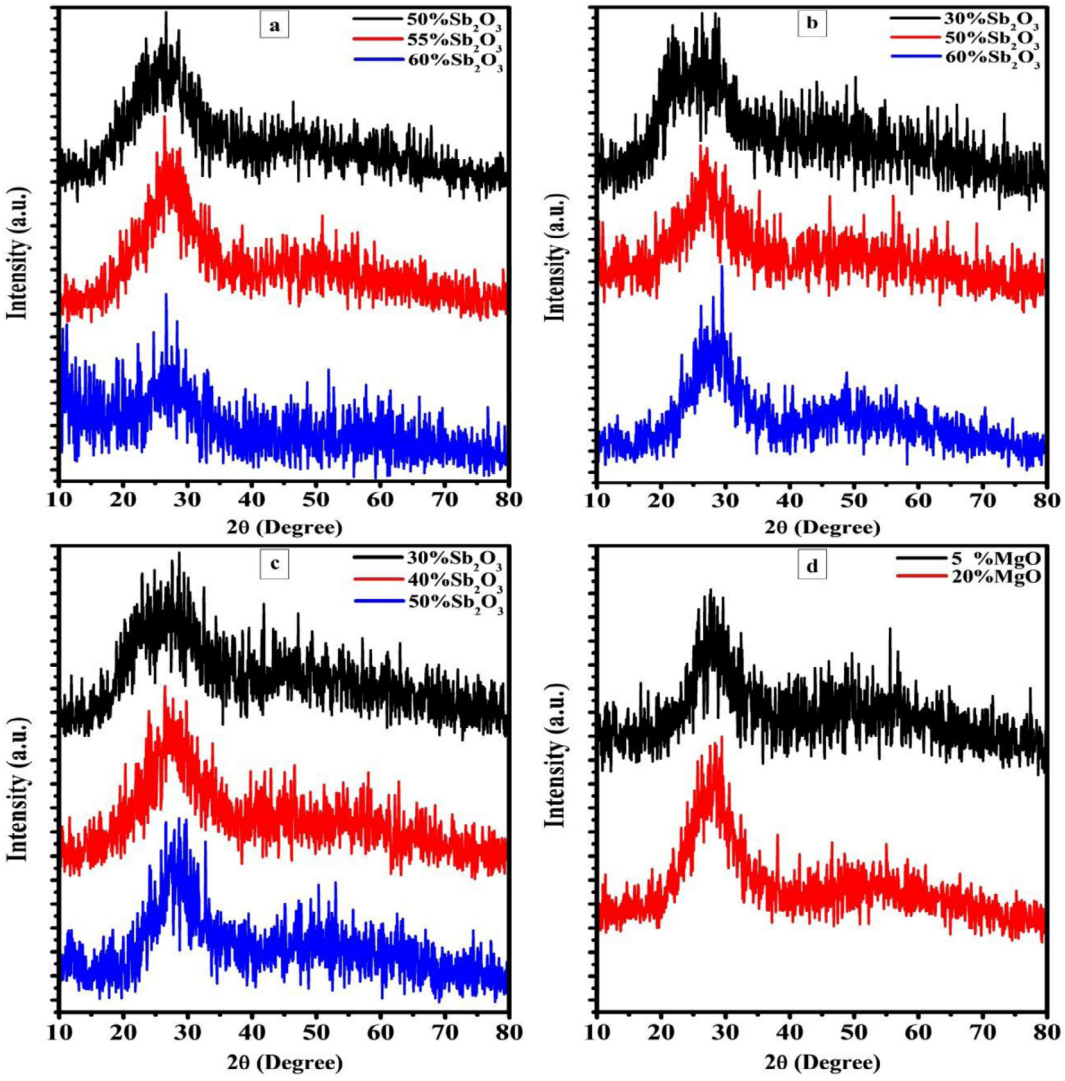

Fig. 2. XRD pattern of: (a) Series I (SPM1, SPM2, and SPM3) (b) Series II (SPM4, SPM5 and SPM6), (c) Series III (SPM7, SPM8 and SPM9), and (d) Series IV (SPM10 and SPM11).

phases with the variation of MgO to Sb_2O_3 molecular ratio [37]. Attempts are made to determine the standard Gibbs energies of magnesium-antimonite phase formation, where pure oxides of MgO and Sb_2O_3 are used [36–40]. It is acknowledged that both MgO and $MgSb_2O_4$ phases together with Sb can coexist in equilibrium [38,39]. Hitherto, fundamental insight of magnesium-antimony-phosphate ternary glass systems is lacking.

In this view, we take an attempt to thrash out the bottleneck of antimony-phosphate based ternary glass research which is a complementary research of our previous study [41], and hope to unravel some basic insight in terms of structure, glass forming ability and thermal stability by synthesizing and characterizing such new glass system. Certainly, for technological applications, comprehensive determination of glass thermal properties is prerequisite. Thus, Sb_2O_3-P_2O_5-MgO ternary glass systems are prepared and inclusive thermal evaluations are made.

Materials and methods

Synthesis

Four series of ternary glasses (Table 1 and Fig. 1) are synthesized via conventional melt quenching technique. High purity analytical grade powdered oxides of Sb_2O_3, P_2O_5, and MgO are selected as raw materials. About 10 gm of constituent materials is thoroughly mixed and pre-treated at 300 °C for 1 h to reduce the presence of bubbles in the mixture and to avoid the volatility of P_2O_5 at high temperature. The mixture was then placed in an alumina crucible before being melted inside a muffle furnace (1050–1100 °C) for 1 h. Upon achieving the desired viscosity the melt is quenched onto a preheated steel plate (300 °C) to form disc-shaped samples before being annealed at 300 °C for 2 h to release the residual stress. The furnace is then switched off and the sample is naturally cooled down to room temperature. Finally, the frozen samples are cut, and polished. Some samples are milled to fine powder for further characterization.

Characterization

The thermal measurement is performed on a Perkin-Elmer Pyris Diamond TG/DTA 7 series system interfaced with built-in computer and software. The highest applied temperature is approximately 1500 °C with the heating rate of 10 °C/min. The temperature difference between the sample (5–10 mg) and the alumina batch is recorded, under controlled nitrogen gas flow (rate 200 ml/min). The DTA traces are obtained, where the glass

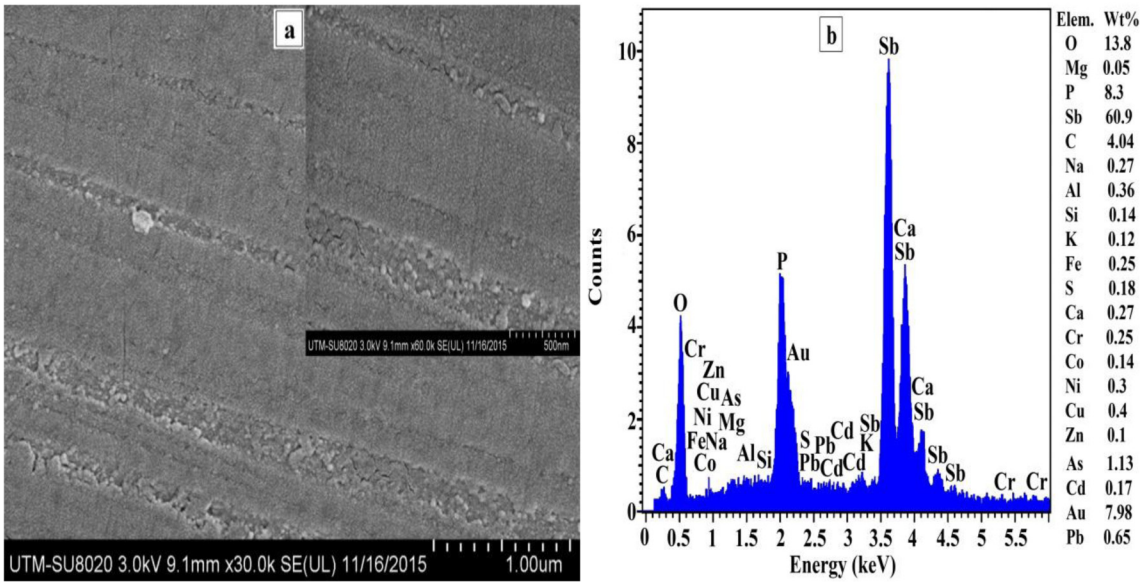

Fig. 3. (a) SEM image of sample SPM3, and (b) the corresponding EDX spectra. The observed discrepancies between the calculated and experimental percentages are due to the placement of sample for prolonged time inside the furnace to acquire the homogeneity at high melting temperature, which led to the volatilization of elements [56,57].

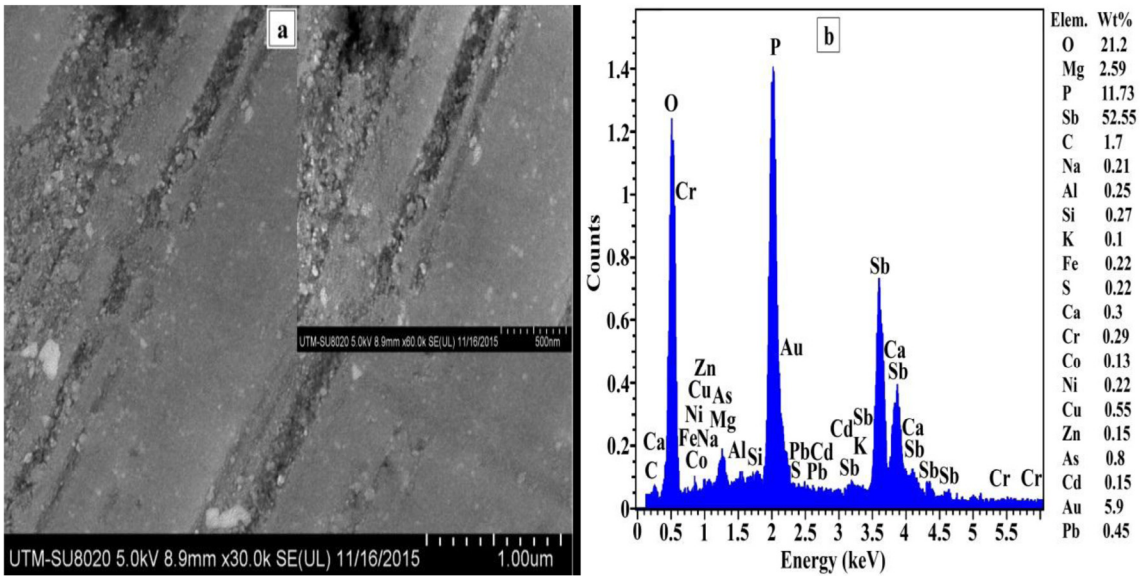

Fig. 4. (a) SEM image of sample SPM4, and (b) the corresponding EDX spectra.

transition temperature (T_g) is identified from intersection of two tangents at the start of the corresponding endothermic peak (kink shape). The onset of crystallization temperature (T_c) is obtained by extrapolating the interception of the first crystallization phase (exothermic reaction) and the highest crystallization temperature (T_p) taken at the maximum of the exothermic reaction. The onset of melting point or solidus temperature (T_s) that separates the solid phase from that of liquid plus crystals is measured from. The offset temperature or liquidus temperature (T_l) which separated the liquid phase from that of liquid plus crystals depending on the derivative heat flow and derivative thermal gravimetric curves.

The glass forming ability (GFA) is calculated through Hurby parameter (H_r) and (ΔT_s). The former one signifies the glass-forming tendency and the later demonstrates the glass stability. The larger value of H_r and ΔT_s (greater 100 °C) implies the greater glass stability against devitrification [40,42]. The expression for H_r and ΔT_s yields:

$$T_s = (T_c - T_g) \tag{1}$$

$$H_r = (T_c - T_g)/(T_l - T_c) \tag{2}$$

The second criteria to identifying the glass forming ability (GFA) depends on the reduced glass transition temperature (T_{rg}). For good glass-forming system the value of T_{rg} must be in the range of $1/2 \leq T_{rg} \leq 2/3$ [43–45]. The value of T_{rg} is calculated via:

$$T_{rg} = \frac{T_g}{T_l} \tag{3}$$

The mass loss is computed using [45,46]:

$$Mass\ loss\ \% = \frac{M_i - M_f}{M_o} \times 100 \tag{4}$$

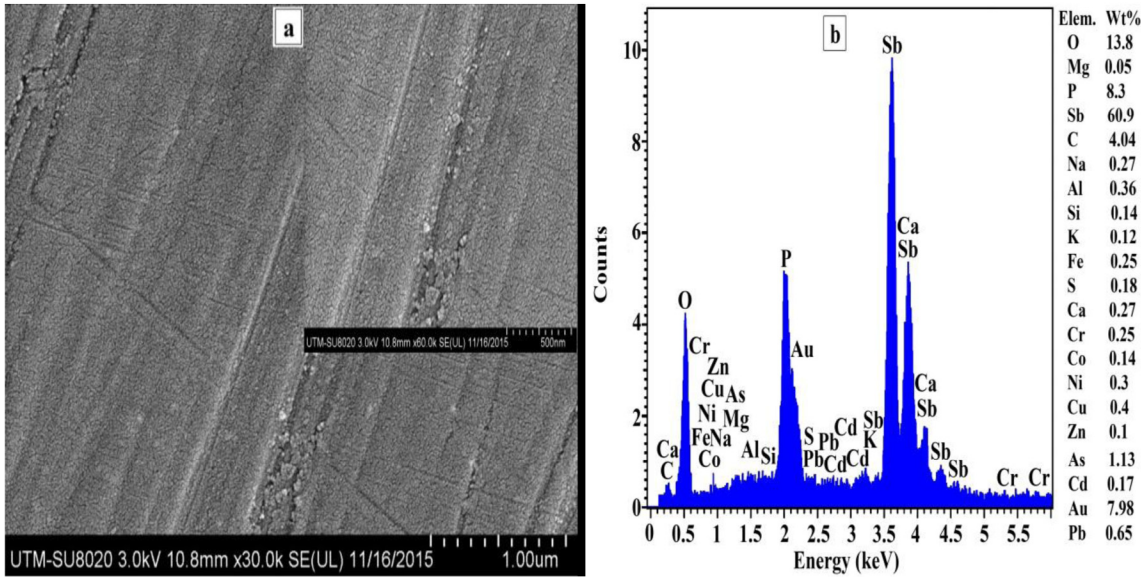

Fig. 5. (a) SEM image of sample SPM9, and (b) the corresponding EDX spectra.3.3 Thermal analysis.

where M_i and M_f are initial and final mass of the sample at the specific temperature range and Mo is the original mass of the sample prior to the thermal analysis.

The amorphous nature and crystalline structure of the prepared samples is confirmed via X-ray diffraction (XRD) (Siemens X-ray Diffractometer D5000). It used Cu-Kα radiation and operated with 40 kV at 30 mA. The diffraction peaks are measured in the 2θ range of 10 to 80° with the step size of 0.05. The glass morphology is imaged using EIGMATm (Zeiss Supra 35 v) field emission scanning electron microscope (FESEM) with accelerating voltages of 5–30 keV. The samples are coated with Au to make them conductive prior to qualitative X-ray microanalysis.

The weight and atomic % of each elemental glass species is estimated using:

$$Weight\,\%\,of\ atom\ (i) = N_i N_o M_i / \sum_i N_i N_o M_i \quad (5)$$

$$Atomic\,\%\,of\ atom\ (i) = N_i N_o / \sum_i N_i N_o \quad (6)$$

where N_i, N_o and M_i represent the atom concentration, number of atom, and atomic mass, respectively for the atom i and i = 1, 2, 3 and 4, stands for Sb, P, Mg and O, respectively.

Results and discussion

XRD analysis

Transparent samples displayed a change in the physical appearance from almost colorless to light yellow and then to deep yellow with increasing Sb_2O_3 and MgO contents. This color variation is ascribed to the emergence of HOMO (Sb 5s and O 2pπ) and LUMO (Sb 5p) gap as well as the presence of the electronic excited states of contaminated cations ion in the visible region [47,48]. Furthermore, the prepared samples with greater than 50 mol% of P_2O_5 and less than 15 mol% of MgO show weak resistance against humidity. The increase in Sb_2O_3 or MgO concentration enhances the resistance against humidity. The lone pair electron of the antimony oxide interacts with water molecules and act as shield. Further addition of MgO as network modifier increase the rupture of the bridging oxygen bonds and thereby protect the network structure from moisture attack [19]. In addition, the prepared samples with high concentration of Sb_2O_3 beyond 60 mol% were opaque, due to crystallization of the samples during preparation. It is worth to mention that the number of lone pair electrons has the profound effect on increasing the glass formation ability [49], but if this number exceeds a certain limit in the structure then the glassy phase is not obtained due to high repulsive interaction among lone pair electrons which may restrain polymerization [49], and it will be confirmed in crystalline phases analysis section. So, the limited glass formation region and low chemical durability could be one of the dilemmas of this ternary glass system.

Fig. 2(a)–(d) shows the XRD pattern of prepared glass samples. The absence of any sharp peak and the presence of broad halo confirmed their amorphous nature.

FESEM analysis

Figs. 3(a), 4(a), and 5(a) show the typical SEM images of a sample from first three series such as SPM3, SPM4, and SPM9, respectively and part (b) displays the corresponding EDX spectra for samples and measured weight% of elements which present the detected elements from experimental (EDX data). SEM micrograph clearly manifested a kind of texture/phase separation (heterogeneous glass) due to liquid-liquid immiscibility of the glass fusible upon quenching from a temperature above T_l to below T_g [5]. The glass separated to more than two textural phases as MgO concentration is increased, which appeared in the form of ribbons, and this is consistent with our previous results, which we explained the effect of external electric field of the ligand group (glass host) on the electronic transitions (absorption or emission) in trivalent rare earth ions and the related spectral shape of these transitions in glasses [41]. The homogeneous and heterogeneous glasses are both entirely vitrified in a macroscopic scale and the difference emerge at the microscopic scale [50], and as known the liquid-liquid immiscibility or micro-phase separation is a common phenomenon which take place in many glass systems and the separation degree depends on the melt viscosity [5]. The extensive experimental results showed that there are many reasons for the occurrence of phase separation phenomena in glass system, like cooling rates, constituents elements number of the glass system, certain additives, modifier cations field strength Z/r^2, tendency to formation

of induced dipoles, degree of coordination required for the modifier cation and the electrostatic interaction between cations in the melt [50–53]. According to the above, there are many factors that govern the formation of micro-phase separation in glass system, and it is difficult to definitely determine the main reason which stands behind the phase separation in antimony phosphate glass system, and the reason could be the intermediates value of MgO modifier cations field strength (0.53) [54] which can tend to form a different shape and size polyhedral from glass former polyhedral which lead to micro-phase separation, another reason could be the incorporation of Sb^{3+} cation with lone electron pair in the glass network which make structural changes in glass network and distortion of SbO_3 unit symmetry [7], [17], [55]. We assume that these structural changes are preceded by structural changes in the fusible glass and form induced dipoles in some structural phases and lead to micro-phase separation.

Thermal analysis

Figs. 6–9 display the DTA traces of all prepared samples categorized into four series. Tables 2 and 3 enlist the detailed thermal properties of these series. Thermal analyses revealed two different values of T_g irrespective of the composition. The first one (weak) occurred at 276 °C and the second one (prominent) around 380–381 °C. However, as the MgO concentration is increased to 25 mol% another T_g is appeared, which is Sb_2O_3 contents dependent. This clearly indicated the modification of amorphous network structure, which is ascribed to the rupture of bridging oxygen (BO) bonds and subsequent formation three types of glass network structure [27,35]. This supported the SEM data, where the existence of inhomogeneous composition in the amorphous state is manifested [25,26,58,59], The T_g value variation in series III (SPM7, SPM8 and SPM9) with increasing Sb_2O_3 content, could be

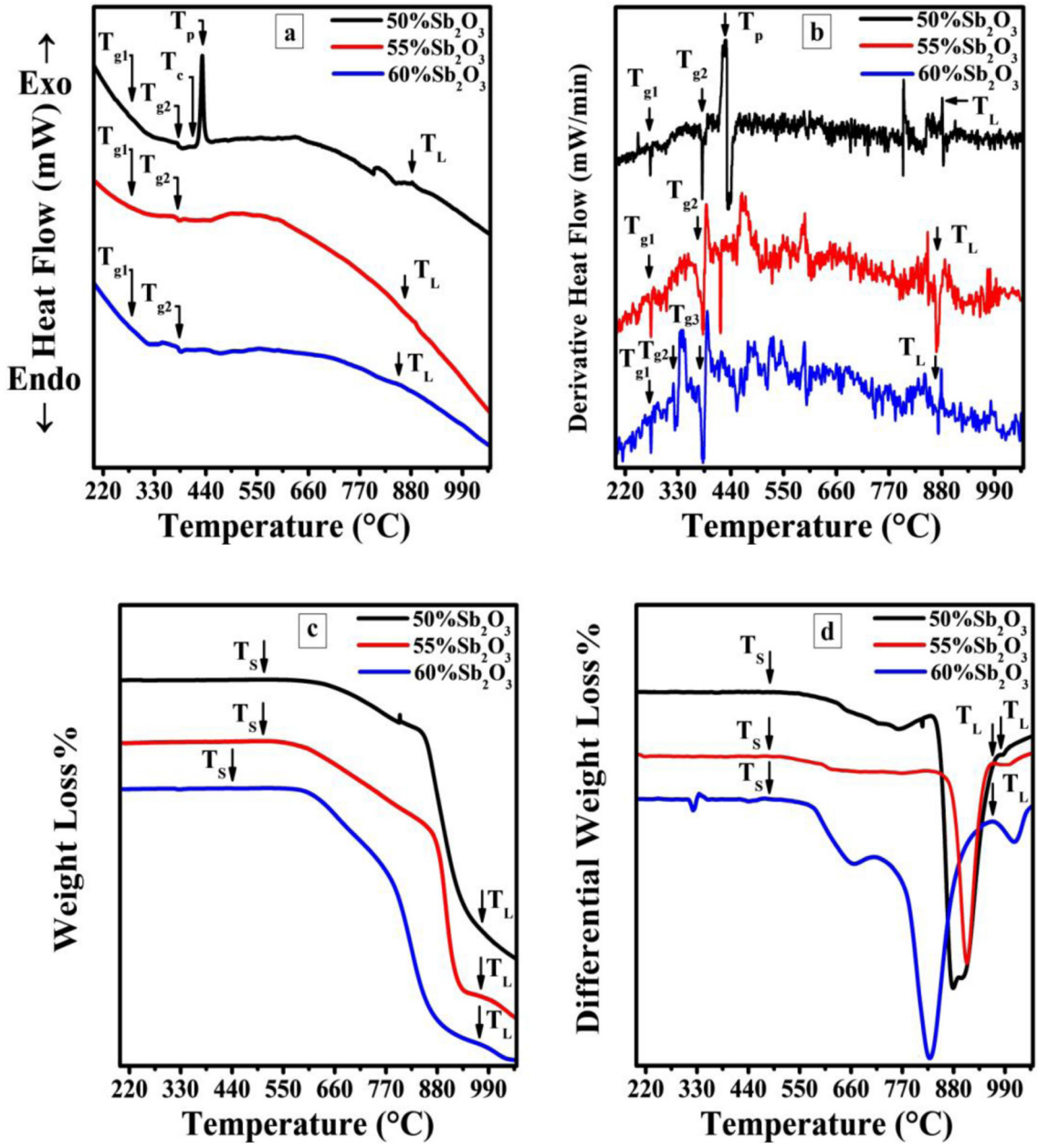

Fig. 6. Samples SPM1, SPM2, and SPM3 (a) heat flow traces, (b) derivative heat flow (c) Weight Loss% (TG curves) and (d) Differential Weight Loss% (DTG curves).

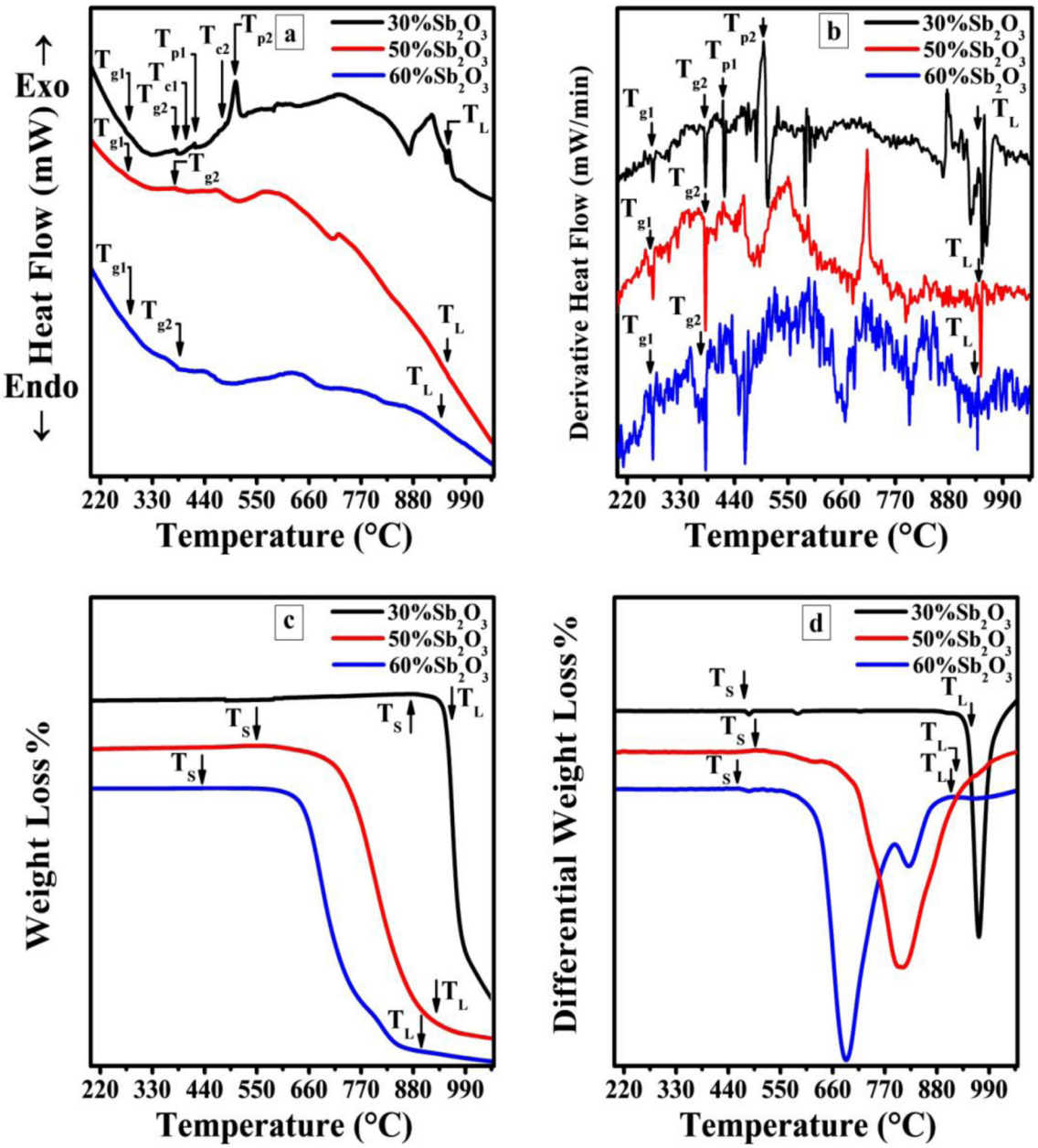

Fig. 7. Samples SPM4, SPM5, and SPM6 (a) heat flow traces, (b) derivative heat flow (c) Weight Loss% (TG curves) and (d) Differential Weight Loss% (DTG curves).

attribute to the average degree of glass polymerization which has a decisive influence on the T_g values [17], the glass sample SPM8 has the largest value of T_g (470 °C) among glass samples, and hence it experienced the highest polymerization rate for the glassy phase. This glass system possessing high-molecular (polymer) character for Sb_2O_3 concentration greater than 50 mol% implies the complete disappearance of both T_c, and T_l. Thus, these glasses are easy to prepare and hard to crystallize. Despite their excellent thermal stability [16] the criterion for large Hruby parameters (H_r) and (ΔT_s) cannot be applied to this glass system [40].

A difficulty is faced to determining the onset of melting point (T_s), and offset temperature (T_l) from the DTA curves due to absence of distinct peak. This is due to the overlap of the endothermic and exothermic peaks. Thus, the derivative heat flow and derivative thermal gravimetric curves are obtained to identify the solidus and liquidus temperature as well the phase formation in this glass system. The disappearance of crystallization temperature peak could be due to the presence of heterogeneous nucleation sites inside the glass matrix need to be clarified. One major reason for the development of sufficient nucleation centre in the glass may be due to the samples exposure to 300 °C (quenching temperature near to T_g) for two hours. This prolonged duration of holding may spontaneously induce the formation of stable crystalline phase by reducing the energy required for the nucleation and growth processes. This is primarily attributed to the glass re-crystallization and subsequent disappearance of sharp peaks in the DTA thermogram. Conversely, it may be ascribed to the too high heating rate, where the rate of nucleation and growth are not rapid enough to follow heating rate. Consequently, the DTA traces (Fig. 6–9) could not detect the re-crystallization or exothermic peak [60,61].

Interestingly, this particular glass system displayed landmarks of melt over a broad temperature range (incongruent melting) at specific composition with increasing Sb_2O_3 and MgO contents. This

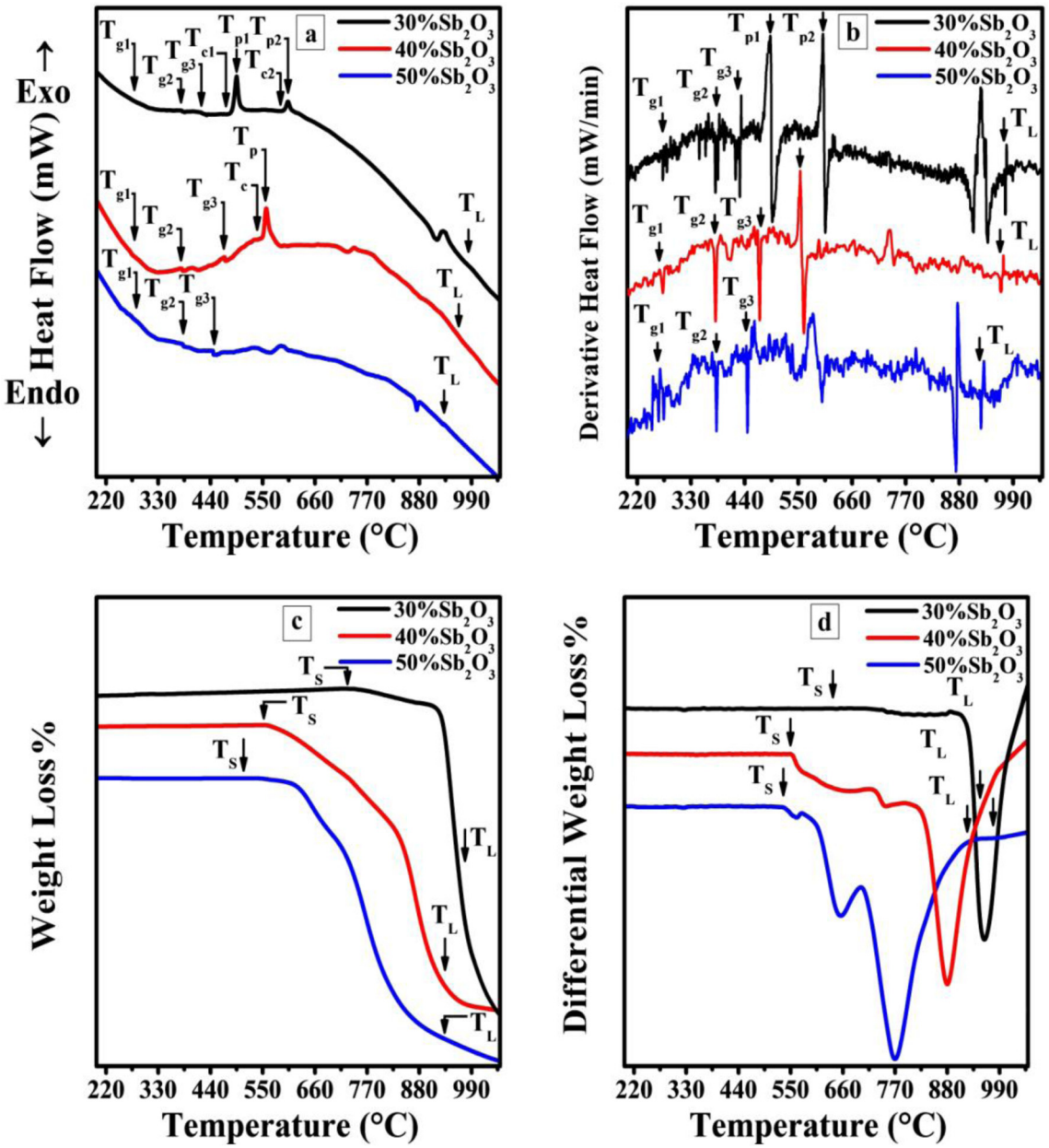

Fig. 8. Samples SPM7, SPM8, and SPM9 (a) heat flow traces, (b) derivative heat flow (c) Weight Loss% (TG curves) and (d) Differential Weight Loss% (DTG curves).

allowed to formation of more phases in this glass system. This glass system melts under stages depending on the phase formation and the heating process. The DTG analysis (endothermic reaction) clearly revealed the melting stages of the crystalline phase and the corresponding weight loss percent due to the vaporization of the crystalline phase at elevated temperature [60,62]. The higher mass loss percent is attributed to the presence of predominant crystalline phase in the disordered matrix and absorption of higher energy. The endothermic reaction is manifested as a sharp peak in the DTA curves, where the SPM4 glass faced the highest (40.7%) mass loss at the final stage of melting. The mass loss for others samples are fairly low at the final stage of melting.

In-depth analyses of the DTG result displayed the occurrence of a clear and distinct inflection point of the baseline, a demarcation of the phase formations that occurred in the glass successively through the heating from the onset of the mass loss. Samples with 5 mol% of MgO with the same solidus temperature (512 °C) encountered many phase changes from the onset of melting (solidus temperature) to the offset of melting (liquidus temperature). The phase formation temperature ranged between 888 and 930 °C encountered higher mass loss percent. This dominant phase among the others phases is observed for the SPM1 and SPM2 samples. Whereas, the phase formation temperature ranging between 780 and 865 °C revealed higher mass loss percent and the dominant phase is seen for SPM3 sample. Samples with 15 and 25 mol % of MgO the solidus temperature is increased with the increase of Sb_2O_3 concentration. Furthermore, the higher mass loss percent at specific temperature range reduced the dominate phase. Samples with 60 mol% of Sb_2O_3 (SPM3, SPM6, SPM10, and SPM11) showed a reduction in the solidus temperature with increasing MgO contents. The occurrence of identical solidus temperature (426 °C) for SPM6, SPM10, and SPM11 samples confirmed the

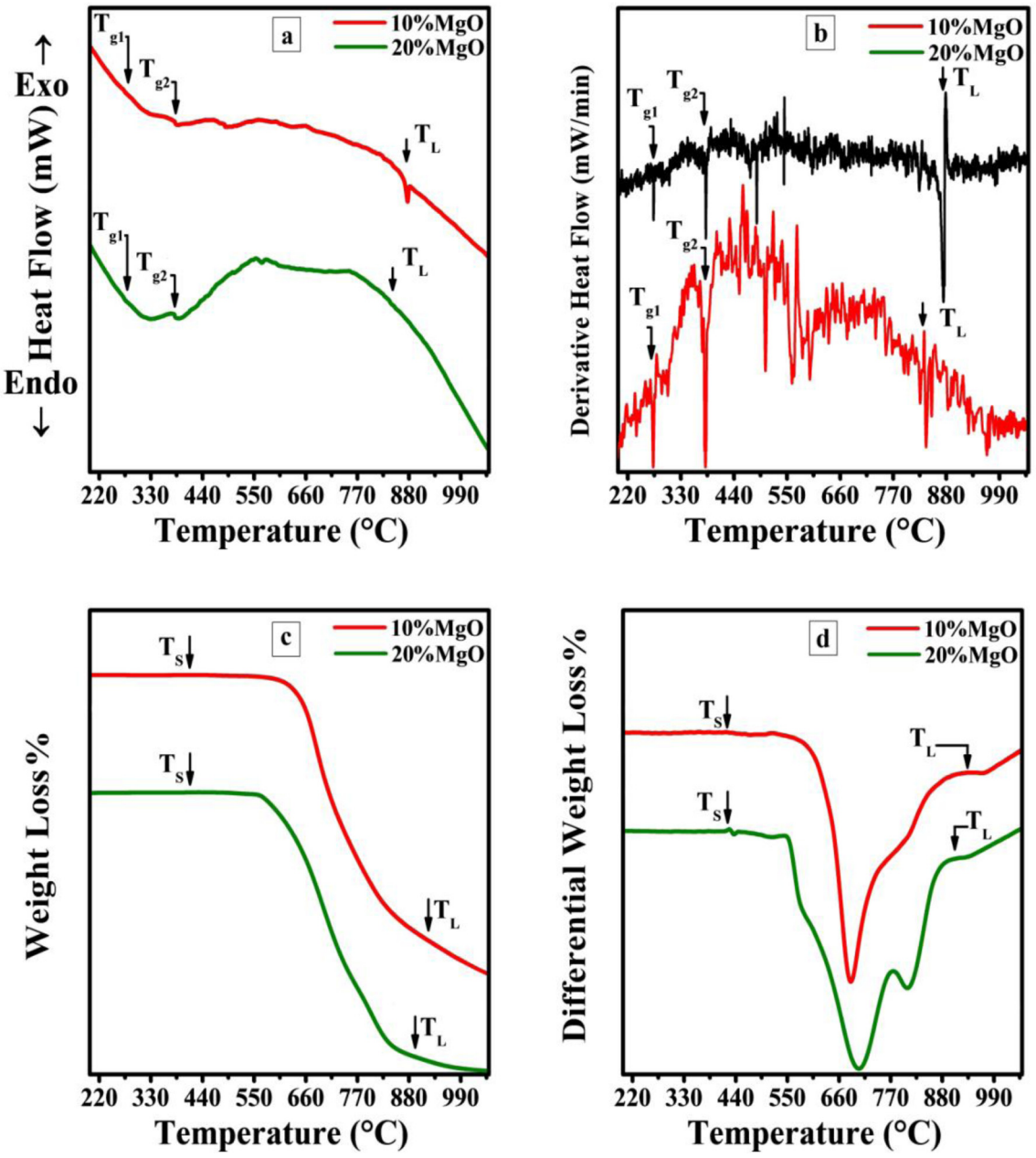

Fig. 9. Samples SPM10, and SPM11 (a) heat flow traces, (b) derivative heat flow (c) Weight Loss% (TG curves) and (d) Differential Weight Loss% (DTG curves).

Table 2
Thermal parameters for all samples.

Temp. (°C) ±2	Glass code										
	SPM1	SPM2	SPM3	SPM4	SPM5	SPM6	SPM7	SPM8	SPM9	SPM10	SPM11
T_g1	276	276	276	276	276	276	276	276	276	276	276
T_g2	381	380	380	381	380	381	381	381	381	381	381
T_g3	–	–	–	–	–	–	422	470	443	–	–
T_c1	423	–	–	417	–	–	488	552.5	–	–	–
T_p1	431	–	–	422	–	–	495	558	–	–	–
T_c2	–	–	–	488	–	–	598	–	–	–	–
T_p2	–	–	–	506	–	–	605.5	–	–	–	–
T_s	512	512	514	880	553	426	726	553.5	500	426	426
T_l	881	875	873	950	945	937	973	965	925	874	836
ΔT_s	42	–	–	36	–	–	66	82.5	–	–	–
H_R	0.091	–	–	0.067	–	–	0.136	0.21	–	–	–
T_g/T_l	0.432	0.434	0.435	0.401	0.402	0.406	0.433	0.487	0.478	0.435	0.455

Table 3
Mass losses on heating for all samples, where Mo: Primary weight in mg, T: Temperature in °C, M_L: Mass loss% and M_r: Final residual mass%.

Parameter	Glass code										
	SPM1	SPM2	SPM3	SPM4	SPM5	SPM6	SPM7	SPM8	SPM9	SPM10	SPM11
M_o	8.72	6.28	7.26	6.97	9.25	9.48	8.36	8.75	8.21	7.05	9.92
Temp. °C	512–630	512–598	512–583	880–914	553–636	426–552	725–885	553–722	500–573	426–518	426–444
(M_L)	(9.1)	(1.7)	(0.4)	(0.27)	(0.97)	(2.1)	(2.3)	(11.0)	(0.49)	(0.28)	(0.1)
Temp. °C	630–795	598–820	583–607	940–997	636–710	552–633	885–917	722–788	573–607	518–603	444–550
(ML)	(9.5)	(17.9)	(9.60)	(40.7)	(2.8)	(2.6)	(0.59)	(7.0)	(0.73)	(0.99)	(0.5)
Temp. °C	795–813	820–845	607–709	–	710–760	633–721	917–975	788–824	607–698	603–645	550–604
(ML)	(5.7)	(1.9)	(12.2)		(8.8)	(42.9)	(32.2)	(4.2)	(13.5)	(5.2)	(5.3)
Temp. °C	813–850	845–888	709–780	–	760–850	721–791	975–985	824–924	698–814	645–722	604–638
(ML)	(2.1)	(7.3)	(10.8)		(36.5)	(18.2)	(5.9)	(34.5)	(38.1)	(25.9)	(6.3)
Temp. °C	850–890	888–920	780–865	–	850–890	791–860	–	924–981	814–865	722–843	638–775
(ML)	(18.4)	(30.8)	(36.3)		(10.0)	(10.5)		(7.3)	(9.9)	(25.8)	(42.0)
Temp. °C	890–930	920–930	865–962	–	910–950	911–986	–	–	865–925	843–891	775–870
(ML)	(21.3)	(6.0)	(10.7)		(3.3)	(1.6)			(5.4)	(4.6)	(17.8)
Temp. °C	930–968	930–957	962–1037	–	–	–	–	–	925–950	891–938	870–918
(ML)	(8.7)	(6.0)	(4.8)						(1.4)	(3.6)	(2.2)
Temp. °C	968–987	957–988	–	–	–	–	–	–	–	–	–
(ML)	(2.50)	(1.20)									
(M_r)	22.70	27.20	15.20	59.0	37.60	22.10	59.0	36.0	30.40	33.6	25.8

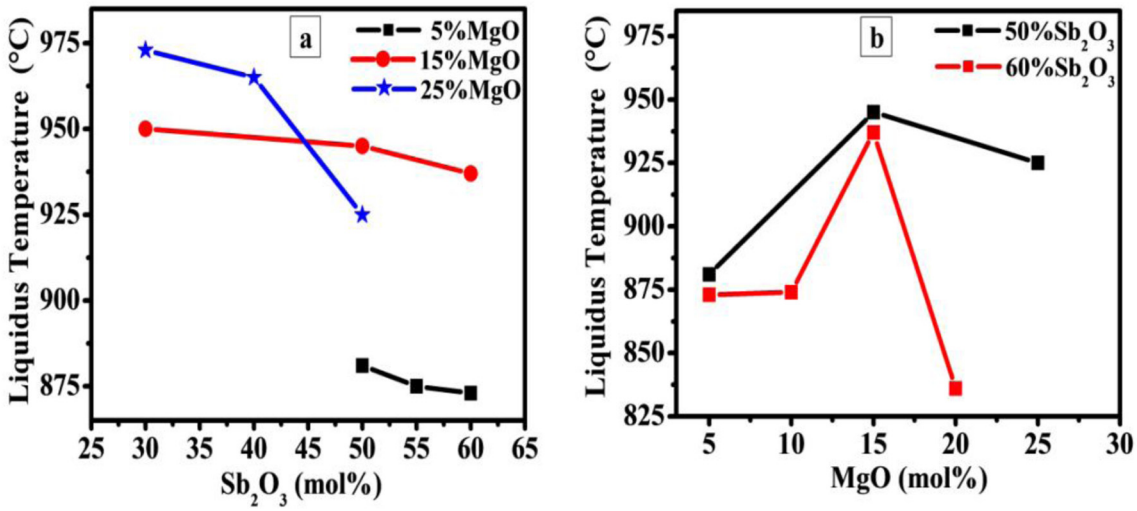

Fig. 10. Concentration (mol%) dependent liquidus temperature (T_l) for varying (a) Sb_2O_3, and (b) MgO.

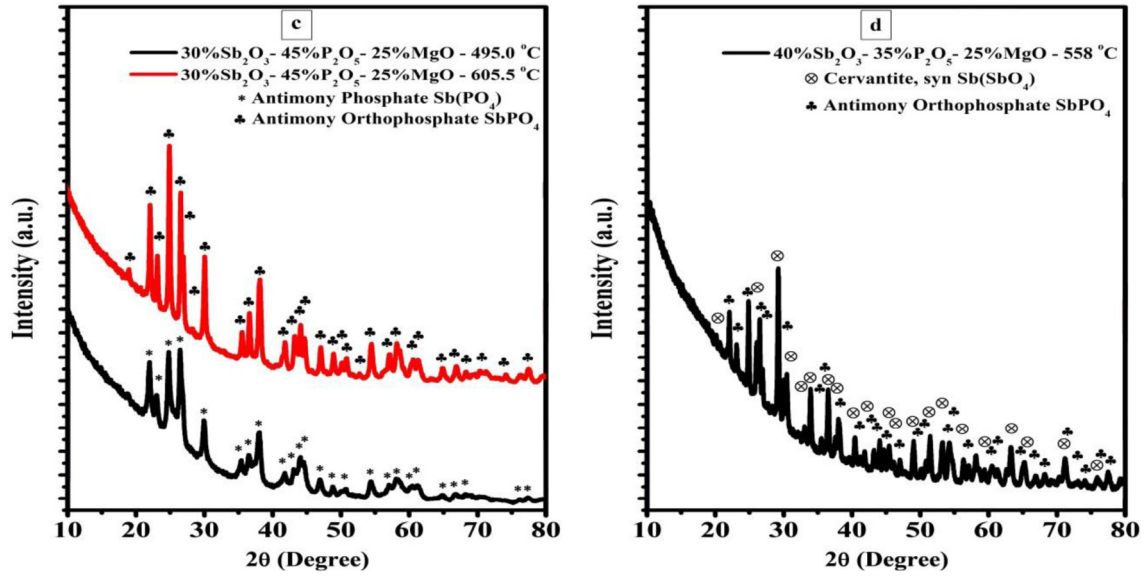

Fig. 11. XRD patterns revealing the sharp crystalline peaks for samples (a) SPM1 (b) SPM4 (c) SPM7 (d) SPM8.

Table 4
Comparison of the present glass thermal properties with other ternary glass system available in the literature.

[Ref.]	Glass composition (mol%)	T_g (°C)	Sag Point (°C)	T_c (°C)	T_l (°C)	$T_c - T_g$ (°C)	H_r	T_g/T_l
[64]	$5K_2O$-$5WO_3$-$90TeO_2$	306	–	416	687	110	0.40	0.44
	$10K_2O$-$20WO_3$-$70TeO_2$	344		509	604	165	1.73	0.56
	$25K_2O$-$25WO_3$-$50TeO_2$	281		419	482	138	2.19	0.58
	$30K_2O$-$40WO_3$-$30TeO_2$	290		377	511	87	0.64	0.76
[65]	30 ZnF2-20 TeO2-50 B2O3	420	–	480	630	60	0.4	0.66
[66]	$70TeO_2$-$27B_2O_3$-3PbO	135.9	–	152.7	173.6	16.8	0.8	0.78
	$70TeO_2$-$21B_2O_3$-9PbO	131.2		157.3	170.2	26.1	2.0	0.77
	$70TeO_2$-$15B_2O_3$-15PbO	128.7		165.7	178.1	37	2.9	0.72
[67]	$80TeO_2$-$5Na_2O$–15MgO	261	–	382	532	121	0.8	0.49
[68]	$15Al_2O_3$-$75P_2O_5$-$10K_2O$	580	–	>900	–	320	–	–
	$20Al_2O_3$-$65P_2O_5$-$15K_2O$	567		814		247		
	17.5Al2O3-62.5P_2O_5-$20K_2O$	526		702		176		
[69]	$5Al_2O_3$-$85B_2O_3$-10BaO	387.7	–	–	–	–	–	
	$10Al_2O_3$-$75B_2O_3$-15BaO	422.8						
	$15Al_2O_3$-$65B_2O_3$-20BaO	512.8						
[70]	$5Al_2O_3$-$90B_2O_3$-$5Li_2O_3$	318.6	–	–	–	–	–	–
	$5Al_2O_3$-$80B_2O_3$-$15Li_2O_3$	426.8						
	$5Al_2O_3$-$70B_2O_3$-$25Li_2O_3$	414.4						
[71]	$60SiO_2$-35BaO-5TiO	–	860	–	1367	–	–	–
	$50SiO_2$-35BaO-15TiO		840		1393			
	$45SiO_2$-35BaO-20TiO		835		1415			
[71]	$70SiO_2$-28BaO-$2La_2O_3$	–	747	–	1355	–	–	–
	$62SiO_2$-33BaO-$5La_2O_3$		775		1305			
	$55SiO_2$-38BaO-$7La_2O_3$		797		1405			
[72]	$30SiO_2$-$30B_2O_3$-40PbO	439		–	–	–	–	–
	$30SiO_2$-20 B_2O_3-50PbO	396	–					
	$30SiO_2$-$10B_2O_3$-60PbO	341						
[73]	$35SiO_2$-44PbO-21 Na_2O	397		551	–	154	–	–
	$40SiO_2$-35PbO-$25Na_2O$	412	–	550–647–780		138		
	$50SiO_2$-25PbO-$25Na_2O$	420		570–650–798		150		
[74]	$45P_2O_5$-$45Na_2O$-10CaO	307	–	434	580	127	0.86	0.52
	$45P_2O_5$-$35Na_2O$-20CaO	336		437–468	660	101	0.45	0.50
	$45P_2O_5$-$15Na_2O$-40CaO	428		543	731	115	0.61	0.58
[75]	$50P_2O_5$-40PbO-$10Ga_2O_3$	432	–	512	712	80	0.4	0.6
	$50P_2O_5$-30PbO-$20Ga_2O_3$	459		544	745	85	0.42	0.61
	$50P_2O_5$-20PbO-$30Ga_2O_3$	448		612	742	164	1.26	0.6
[76]	$50P_2O_5$-48BaO-$2CaF_2$	428	–	543	831	115	0.399	0.51
	$50P_2O_5$-44BaO-$6CaF_2$	440		563	824	123	0.471	0.53
	$50P_2O_5$-40BaO-$10CaF_2$	444		575	801	131	0.580	0.55
Ours	$50Sb_2O_3$-$45P_2O_5$-5MgO	276–381	–	423	976	42	0.075	0.390
	$55Sb_2O_3$-$40P_2O_5$-5MgO	276–380		–	974	–	–	0.390
	$60Sb_2O_3$-$35P_2O_5$-5MgO	276–380		–	971	–	–	0.390
	$30Sb_2O_3$-P_2O_5-15MgO	276–381		417–488	952	36	0.060	
	$50Sb_2O_3$-P_2O_5-15MgO	276–381		–	922	–	–	0.400
	$60Sb_2O_3$-P_2O_5-15MgO	276–381		–	911	–	–	0.412
	$30Sb_2O_3$-$45P_2O_5$-25MgO	276–381–422		488–598	980	66	0.130	0.418
	$40Sb_2O_3$-$35P_2O_5$-25MgO	276–381–470		552.5	934	82.5	0.210	0.430
	$50Sb_2O_3$-$25P_2O_5$-25MgO	276–381–443		–	932	–	–	0.500
	$60Sb_2O_3$-$30P_2O_5$-10MgO	276–381		–	921.5	–	–	0.470
	$60Sb_2O_3$-$20P_2O_5$-20MgO	276–381		–	896	–	–	0.410
								0.420

encounter of eutectic reaction. This is supported by the emergence of the onset crystallization temperature (423 °C) for sample SPM1.

More interestingly, within the same sample series the solidus and liquidus temperature is found to decrease with increasing Sb_2O_3 contents, this result unambiguously manifest that Sb_2O_3 incorporation in the glass matrix made a significant structural change in the glass network and it is same results reached by Koudelka and Zhang [17,19], the incorporation of Sb_2O_3 at low concentration lead to depolymerisation of phosphate chains and formation of isolated pyramidal SbO_3 structural units with a lone-pair on the Sb atom, with increasing Sb_2O_3 content lead to increases the isolated SbO_3 units linking into chains and clusters with Sb–O–Sb bonds [17], the pyramidal SbO_3 unit with lone electron pair has a greater angular volume compared with a bonding pair of electrons and its involvement in the glass network lead to decrease in the symmetric of Sb^{3+} local structure and the glass network strain energy will be increases, and hence the additional activation energy decreases which is requisite for rearrangement of the glass network [19,63], Thus, T_s and T_l of the glasses decrease with increasing Sb_2O_3 concentration.

However, samples series with 15 and 25 mol% of MgO have the highest liquidus temperature than series with 5 mol% of MgO as shown in the Fig. 10(a), and the liquidus temperature revealed a decrement with increasing Sb_2O_3 contents, while increases with increasing MgO contents till 15 mol% and then decrease as shown in the Fig. 10(a) and (b) respectively. The occurrence of lowest liquidus temperature (836 °C) for sample SPM11 is because of the closeness of eutectic reaction of this system.

Table 4 compares the thermal properties of some well-studied ternary system with the present antimony phosphate magnesium glass system. In some cases, all the thermal parameters data are not available. It is clear that the values of T_g, T_c, T_p, T_s, and T_l of a glass system is mainly decided by the type of glass former, modifier, and their concentration in the system. The present antimony phosphate magnesium glass system thermal parameters are comparable to the tellurite and borate glass systems. Furthermore, this

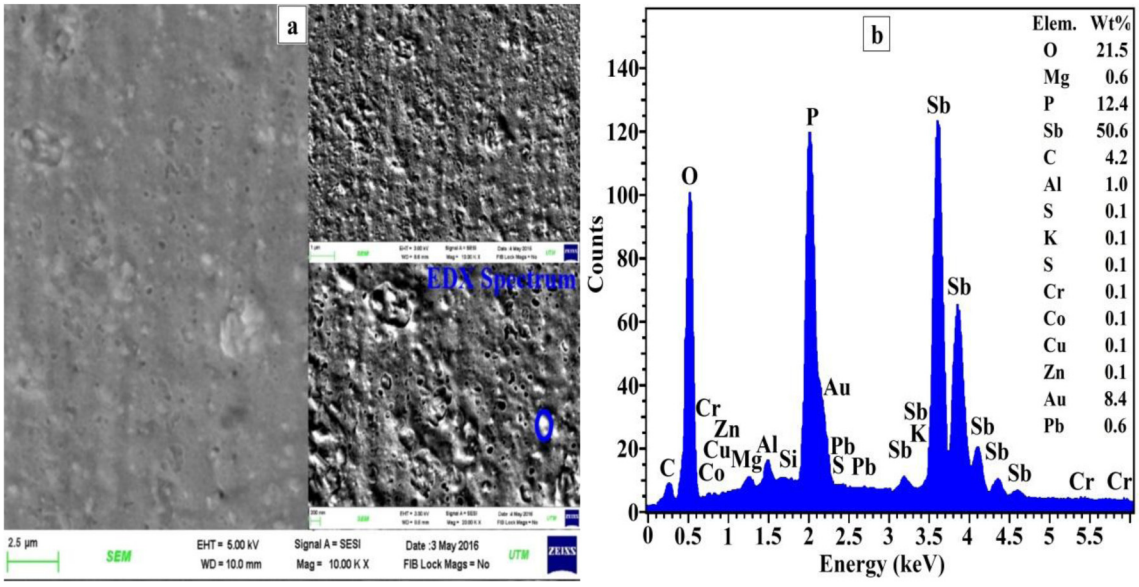

Fig. 12. (a) FESEM image of sample SPM1 (T_p = 431 °C), and (b) the corresponding EDX spectra for selected area.

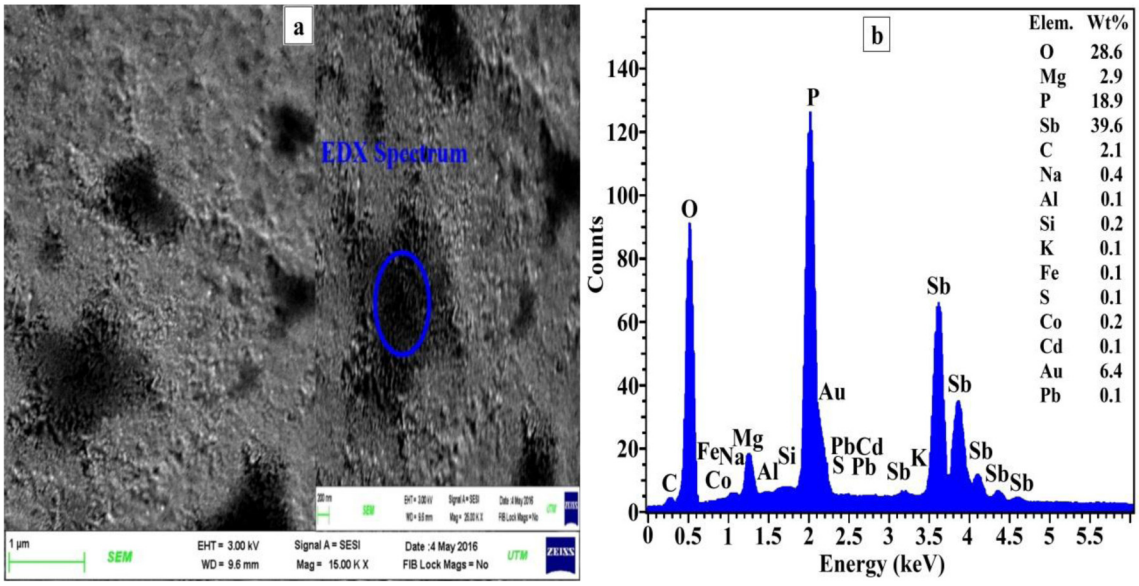

Fig. 13. (a) FESEM image of sample SPM4 (T_p = 422 °C), and (b) the corresponding EDX spectra for selected area.

glass system shows inhomogeneous composition in terms of phase separation (heterogeneous glass), multiple T_g values and high-molecular polymer character (excellent thermal stability), which are not the signature for other types of ternary glasses. These modulations of glass properties are highly advantageous for the advance optoelectronic applications.

Crystalline phases analysis

In order to investigate the crystalline phases in this glass system, samples SPM1, SPM4, SPM7 and SPM8 have been chosen which revealed crystallization temperature peak in the DTA traces. The crystallization process of the samples are carried out by annealing the bulk and powdered glass samples at their respective crystallization temperature, T_p for 24 h in an electrical furnace. The bulk samples are finally polished until scratch-free under light microscope to prepare them for FE-SEM image. The annealing temperature for SPM1 is (431 °C), SPM4 is (422 °C and 506 °C), SPM7 is (495 °C and 605.5 °C) and SPM8 is (558 °C). The crystalline structural phases and their morphological are identified by using powder X-ray diffraction (XRD) and field emission scanning electron microscopy (FE-SEM), respectively. All samples appeared opaque after annealing process except sample SPM7 – 495 °C which appeared semi-crystalline. Figs. 11(a)–(d) and 12(a), (b), 13(a), (b), 14(a), (b), 15(a), (b), 16(a), (b), and 17(a), (b) show the powder X-ray diffraction patterns of the crystalline samples and the typical SEM images of the crystalline sample and corresponding EDX spectra for selected area respectively. For sample SPM1 – 431 °C the only phase was identified was antimony phosphate $Sb(PO_4)$ which matched with ICDD (PDF-2-01-071-2275, Release 2015 RDB). For sample SPM4 – 422 °C the major phase was antimony phosphate $Sb(PO_4)$ which matched with ICDD (PDF-2-01-071-2275, Release 2015 RDB) and the minor phase was magnesium phosphate $Mg(PO_3)_2$ which matching with ICDD (PDF-2-00-027-1273, Release

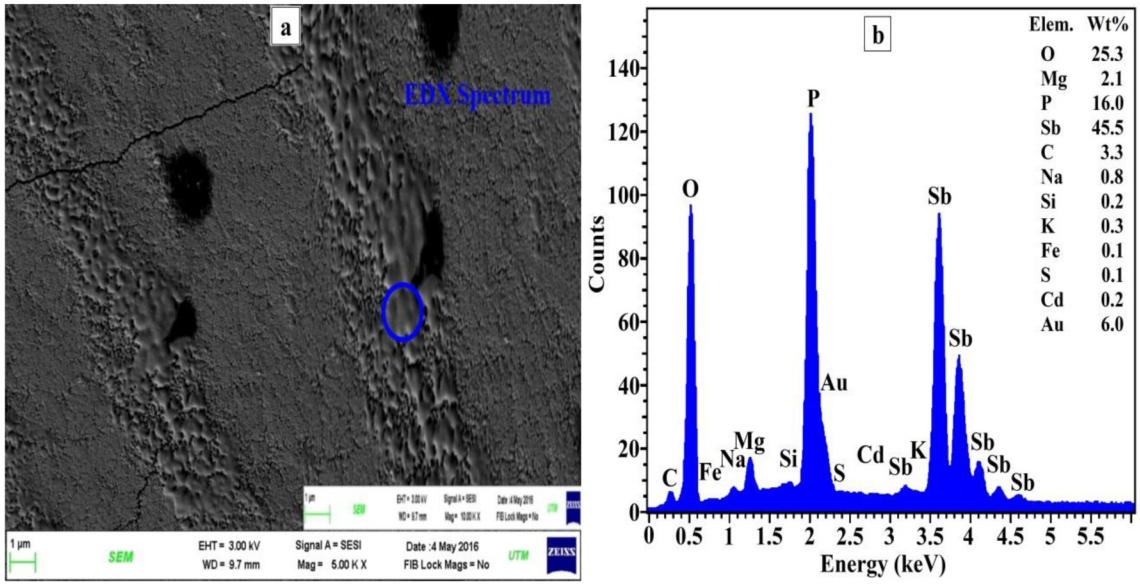

Fig. 14. (a) FESEM image of sample SPM4 (T_p = 506 °C), and (b) the corresponding EDX spectra for selected area.

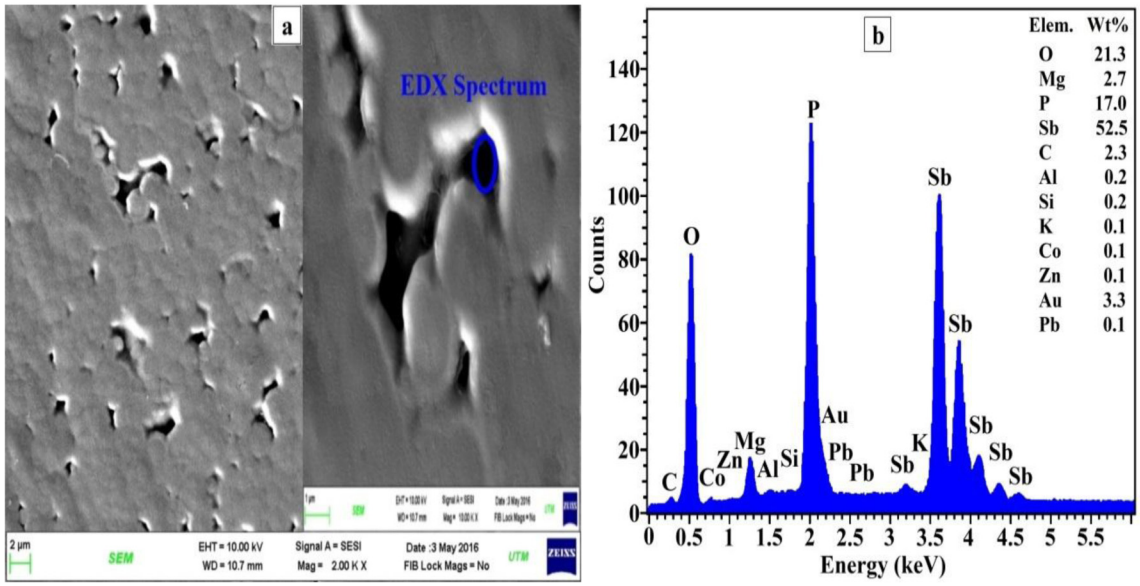

Fig. 15. (a) FESEM image of sample SPM7 (T_p = 495 °C), and (b) the corresponding EDX spectra for selected area.

2015 RDB). For sample SPM4 – 506 °C the major phase was antimony orthophosphate SbPO4 which matched with ICDD (PDF-2-01-078-1791, Release 2015 RDB) and magnesium cyclo-tetraphosphate $Mg_2P_4O_{12}$ as the minor phase which matched with ICDD (PDF-2-01-070-1803, Release 2015 RDB). For sample SPM7 – 495 °C the major phase was antimony phosphate $Sb(PO_4)$ which matched with ICDD (PDF-2-01-071-2275, Release 2015 RDB). For sample SPM7 – 605.5 °C the major phase was antimony orthophosphate $SbPO_4$ which matched with ICDD (PDF-2-01-078-1791, Release 2015 RDB). For sample SPM8 – 558 °C the major phase was antimony orthophosphate $SbPO_4$ which matched with ICDD (PDF-2-01-078-1791, Release 2015 RDB), and the minor phase was cervantite, syn $Sb(SbO_4)$ which matched with ICDD (PDF-2-01-078-2066, Release 2015 RDB). In addition, the major phase in the crystalline samples is antimony phosphate at temperature below 500 °C and antimony orthophosphate at temperature higher than 500 °C as shown in the XRD analysis, summarized in Table 5. It is also found that the MgO modifier had an impact on the phase occurrence where if its concentration is higher than 5 mol% (as 15 and 25 mol%) a new minor phases as magnesium phosphate and magnesium cyclo-tetraphosphate (at 55 mol% of P_2O_5), and Cervantite, syn (at 40 mol% of Sb_2O_3) were emerged. According to the ICDD (PDF-2-) card, there is no difference between antimony phosphate $Sb(PO_4)$ and antimony orthophosphate $SbPO_4$ in terms of crystal structure, they have the same monoclinic crystal system and belong to (P21/m) space group, the only difference is in the edges lengths of the unit cell (a, b, c), which leads to different unit cell volume and density, for both compounds antimony phosphate and antimony orthophosphate, which are (161.80 $Å^3$, 4.448 g/cm^3) and (162.00 $Å^3$, 4.443 g/cm^3) respectively. The same case with magnesium phosphate $Mg(PO_3)_2$ and magnesium cyclo-tetraphosphate $Mg_2P_4O_{12}$ both have monoclinic crystal structure

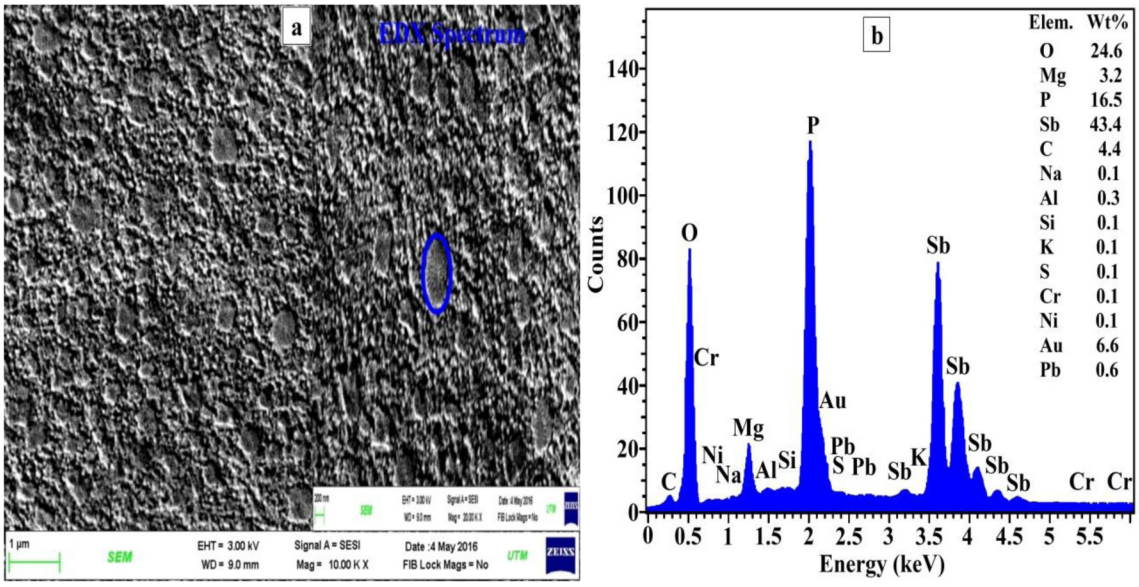

Fig. 16. (a) FESEM image of sample SPM7 (T_p = 605.5 °C), and (b) the corresponding EDX spectra for selected area.

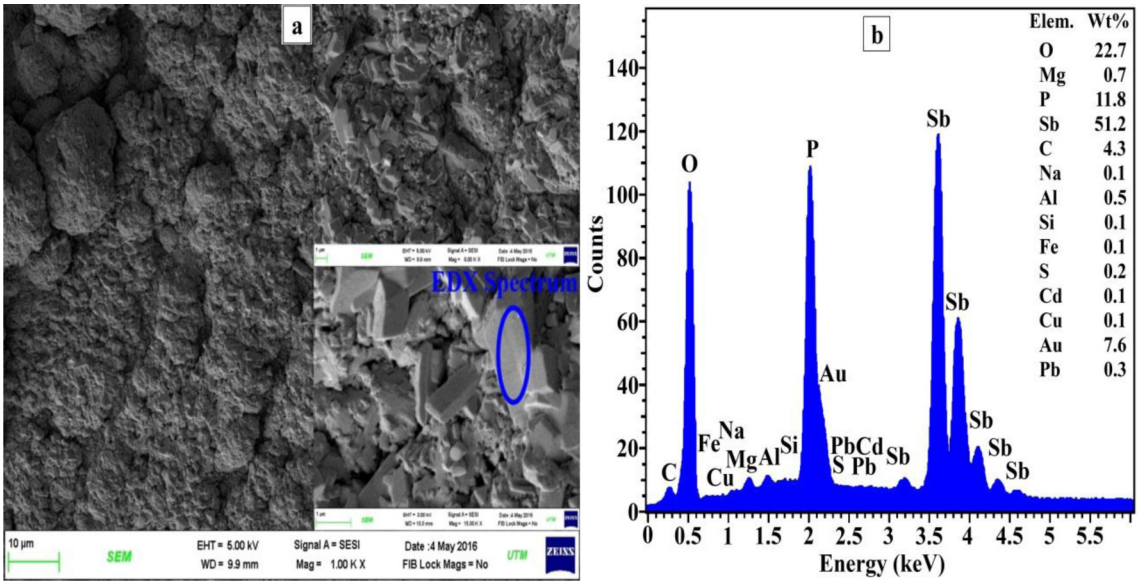

Fig. 17. (a) FESEM image of sample SPM8 (T_p = 558 °C), and (b) the corresponding EDX spectra for selected area.

and their data are (842.91 Å^3, 2.872 g/cm^3) and (845.12 Å^3, 2.86 g/cm^3) respectively. For the cervantite $Sb(SbO_4)$ phase which belong to orthorhombic crystal structure and Pna21 space group 307.82 Å^3 and 6.635 g/cm^3. The presence of three peculiar crystalline phases which are antimony phosphate $Sb(PO_4)$, antimony orthophosphate $SbPO_4$ (major crystalline phases) and cervantite $Sb(SbO_4)$ (minor crystalline phase) which known as distinct polymorph of antimony tetroxide Sb_2O_4 [77], these crystalline phases possess the lone pair property ($5s^2$) in their structures and have large non-linear optical susceptibility coefficient (χ^3) [47] and possess a large impact on the glass optical properties [6,77]. The outstanding features of the lone pair electron inside glass matrix are the flexibility character (easy to deform) of the lone pair electron, structure with lone pair produces less strain energy during amorphous polyhedra formation and strong steric effects due to interaction among lone pair electrons (electrostatic repulsion) [49]. The presence of this lone pair enhances the nonlinear optical susceptibility in the antimonite glasses described by third rank polar tensors [78]. Furthermore, the existence of different crystalline phases in this ternary glass system can modify the rare earth spectroscopic properties in terms of electronic transitions (absorption or emission) and the related spectral shape of these transitions in this glass matrix, which can be done through stark effect results from the presence of an external electric field of the ligand group (glass host) around the active ions which leads to spectral lines splitting and shifting of the active ions, and each stark level has a specific energy and a specific width [79–81]. So, trivalent rare earth elements inside glass with multi-crystalline phases might experience different local electric and magnetic fields so the transitions spectral shape is from the different type of stark level structure, and lead to manipulate the rare earth spectroscopic properties.

Table 5
XRD analysis of various crystalline phases for four selected samples.

XRD analysis	Samples					
	SPM1 (431 °C)	SPM4 (422 °C)	SPM4 (506 °C)	SPM7 (495 °C)	SPM7 (605.5 °C)	SPM8 (558 °C)
Major Crystalline Phase	Antimony Phosphate	Antimony Phosphate	Antimony Orthophosphate	Antimony Phosphate	Antimony Orthophosphate	Antimony Orthophosphate
Minor Crystalline Phase	–	Magnesium Phosphate	Magnesium cyclo-tetraphosphate	–	–	Cervantite, syn
Major Crystallite size (Å)	159.7	345.2	432	110.2	169.9	272.8
Minor Crystallite size (Å)	–	456.4	237.4	–	–	366
Major Phase Weight (%)	100	70.2	65.4	100	100	55.8
Minor Phase Weight (%)	–	29.8	34.6	–	–	44.2

Conclusions

Four series of magnesium-antimony-phosphate glasses of new compositions are synthesized and thermal properties are determined as a function of varying modifiers concentrations. Glass transition temperature, crystallization temperature, thermal stability, solidus temperature, and liquidus temperature are systematically measured and their origin is explained via various mechanisms. Glasses are found to be transparent, and thermally stable with inhomogeneous textural morphology. The SEM images manifested their phase formation (heterogeneous glass) and EDX spectra detected the accurate elemental traces in the presence of contamination from furnace heating elements and crucible materials. Glasses with 50 mol% of Sb_2O_3 exhibited excellent thermal stability, displaying landmarks of melt over a broad temperature range (incongruent melting). Furthermore, these glass systems encountered many phases from the onset of melting (solidus temperature). The number of phase formation possibility is enhanced with increasing Sb_2O_3 and MgO modifiers content. Glass sample with composition of $60Sb_2O_3$-$20P_2O_5$-20MgO showed lowest liquidus temperature (836 °C) and solidus temperature (426 °C) among all other samples due to eutectic reaction, also the emergence of five crystalline phases in the area studied of ternary diagram gave an evidence that this oxide system encounter many phase transition through the concentration or temperature changes. Our careful experimental evaluation on thermal properties in magnesium-antimony-phosphate glasses may contribute towards the development of phosphate glass based device fabrication and non-linear optical material.

Acknowledgements

The authors gratefully acknowledge the financial support from UTM and Malaysian Ministry of Education through GUP (Vot. 05H36, 05H42, and 05H45) and FRGS (Vot. 4F424, and 4F319). Soham Younis Moustafa is grateful to Ministry of Higher Education and Scientific Research of Iraq Republic for providing the doctoral scholarship.

References

[1] Yamane M, Asahara Y. Glasses for photonics. Cambridge University Press; 2000.
[2] Hirao K, Mitsuyu T, Si J, Qiu J. Active glass for photonic devices: photoinduced structures and their application, vol. 7. Springer Science & Business Media; 2013.
[3] Gonella F, Mazzoldi P. Metal nanocluster composite glasses. In: Nalwa HS, editor. Handbook of nanostructured materials and nanotechnology, vol. 4. San Diego: Academic Press; 2000.
[4] Prasad PN. Nanophotonics. New Jersey: Wiley; 2004.
[5] Shelby JE. Introduction to glass science and technology. Royal Society of Chemistry; 2005.
[6] Melnikov P, dos Santos HWL, Gonçalves RV. Thermal behavior of the mixed composition xSb_2O_3–$(1-x)$ Bi_2O_3–$6(NH_4)$ $2HPO_4$. J Therm Anal Calorim 2010;101(3):907–11.
[7] Sahar MR, Ahmed MM, Holland D. The crystallisation of Sb_2O_3-$PbCl_2$- $ZnCl_2$ glasses. Phys Chem Glasses 1990;31(3):126–31.
[8] Sahar MR, Holland D. Chemical durability of oxychloride glasses. J Non-Cryst Solids 1992;140:107–11.
[9] De Araújo CB, Boudebs G, Briois V, Pradel A, Messaddeq Y, Nalin M. Nonlinear refractive index measurements in antimony-sulfide glass films using a single beam nonlinear image technique. Opt Commun 2006;260(2):723–6.
[10] Kelly GD. U.S. Patent No. 3,002,842. Washington, DC: U.S. Patent and Trademark Office; 1961.
[11] Nalin M, Poulain M, Poulain M, Ribeiro SJ, Messaddeq Y. Antimony oxide based glasses. J Non-Cryst Solids 2001;284(1):110–6.
[12] Hidden WA, King BW. Antimony oxide glasses. J Am Ceram Soc 1956;39 (6):218–22.
[13] Winter A. Les verres transparents dans l'infrarouge: les oxydes. Verres Refract 1982;36:353–6.
[14] Soltani MT, Boutarfaia A, Makhloufi R, Poulain M. New alkali antimonate glasses. J Phys Chem Solids 2003;64(12):2307–12.
[15] Baazouzi M, Soltani MT, Hamzaoui M, Poulain M, Troles J. Optical properties of alkali-antimonite glasses and purified processes for fiber drawing. Opt Mater 2013;36(2):500–4.
[16] Qi Y, Wang Z, Zhai S, Jiang S, Lin H. Study of structures and properties of ZnO-Sb_2O_3-P_2O_5-Na_2O glasses. Mater Sci Poland 2014;32(3):414–8.
[17] Koudelka L, Šubčík J, Mošner P, Montagne L, Delevoye L. Structure and properties of Sb_2O_3-containing zinc borophosphate glasses. J Non-Cryst Solids 2007;353(18):1828–33.
[18] Ghosh A, Chaudhuri BK. Anomalous conductivity and other properties of V_2O_5-P_2O_5 glasses with Bi_2O_3 OR SbO_3. J Non-Cryst Solids 1988;103(1):83–92.
[19] Zhang B, Chen Q, Song L, Li H, Hou F. The influence of Sb_2O_3 addition on the properties of low-melting ZnO-P_2O_5 Glasses. J Am Ceram Soc 2008;91 (6):2036–8.
[20] Sudarsan V, Kulshreshtha SK. Study of structural aspects of PbO-P_2O_5-Sb_2O_3 glasses. J Non-Cryst Solids 2001;286(1):99–107.
[21] Hudgens JJ, Brow RK, Tallant DR, Martin SW. Raman spectroscopy study of the structure of lithium and sodium ultraphosphate glasses. J Non-Cryst Solids 1998;223(1):21–31.
[22] Karakassides MA, Saranti A, Koutselas I. Preparation and structural study of binary phosphate glasses with high calcium and/or magnesium content. J Non-Cryst Solids 2004;347(1):69–79.
[23] Ding GH, Xie W, Jung IH, Qiao ZY, Du GW, Cao ZM. Thermodynamic assessment of the MgO-P_2O_5 and CaO-P_2O_5 Systems. Acta Phys Chim Sin 2015;31(10):1853–63.
[24] Berak J. The system magnesium oxide – phosphorus pentoxide. Roczniki Chemii 1958;32:17–22.
[25] Iwase M, Akizuki H, Fujiwara H, Ichise E, Yamada N. A thermodynamic study of MgO-P_2O_5 slags by means of solid-oxide galvanic cell at 1673-K. Steel Res 1987;58(5):215–9.
[26] Sarver JF, Hummel FA. Phase equilibria and fluorescence in the system Zn $(PO_3)_2$-$Mg(PO_3)_2$. J Electrochem Soc 1959;106(6):500–4.
[27] Abdelkader SB, Cherifa AB, Khattech I, Jemal M. Synthèse, caractérisation et thermochimie du phosphate trimagnésien et du phosphate tricalcique. Thermochim Acta 1999;334(1):123–9.
[28] Czupinska G. The system YPO_4-$Mg_3(PO_4)_2$-$Mg_2P_2O_7$. J Therm Anal 1992;38 (10):2343–7.
[29] Calvo C, Leung JS, Datars WR. ESR Study of Mn^{2+} in α-and β-$Mg_2P_2O_7$. J Chem Phys 1967;46(2):796–803.
[30] Serazetdinov DZ, Poletsev EV, Kushnikov Y. Characteristic features of the formation of crystalline magnesium tetrametaphosphate. Russ J Inorg Chem 1967;12(11):1599–600.
[31] Czupińska G. Phase equilibria in the system YPO_4-$Mg(PO_3)_2$. Thermochim Acta 1992;202:77–80.
[32] Meyer K, Hobert H, Barz A, Stachel D. Infrared spectra and structure of various crystalline ultraphosphates and their glasses. Vib Spectrosc 1994;6(3):323–32.
[33] Jung IH, Hudon P. Thermodynamic assessment of P_2O_5. J Am Ceram Soc 2012;95(11):3665–72.
[34] Greenwood NN, Earnshaw A. Chemistry of the elements. Elsevier; 2012.
[35] Sahar MR, Kamaruddin N. A study on the phase transformation of MgO-P_2O_5 glass by X-ray diffraction. School of Materials and Mineral Resources Engineering Universiti Sains Malaysia, Perak Branch Campus 31750 Tronoh, Perak, Malaysia, 233; 1996.

[36] Sukhomlinov D, Aspiala M, Taskinen P. Thermodynamic study of MgO-Sb_2O_3 system and the stability functions of magnesium antimonite. J Chem Thermodyn 2014;72:71–6.
[37] Ropp RC. Encyclopedia of the alkaline earth compounds. Newnes; 2012.
[38] Kemori N, Denholm WT, Saunders S. Measurements of standard Gibbs energies of formation of Sb_2O_3, $MgSb_2O_4$ and $Ca_4Sb_2O_7$ by an EMF method. Can Metall Q 1996;35(3):269–74.
[39] Katayama I, Sugimura S, Kozuka Z. Measurements of standard molar Gibbs energies of formation of Sb_2O_3, $ZnSb_2O_4$ and $MgSb_2O_4$ by EMF method with zirconia solid electrolyte. Trans Jpn Inst Metals 1987;28(5):406–11.
[40] Hrubý A. Evaluation of glass-forming tendency by means of DTA. Czechoslovak J Phys B 1972;22(11):1187–93.
[41] Moustafa SY, Sahar MR, Ghoshal SK. Erbium ions oscillator strength and emission enhancement in antimony phosphate amorphous matrix. J Non-Cryst Solids 2016;433:87–94.
[42] Jlassi I, Elhouichet H, Ferid M. Thermal and optical properties of tellurite glasses doped erbium. J Mater Sci 2011;46(3):806–12.
[43] Turnbull D. Under what conditions can a glass be formed? Contemp Phys 1969;10(5):473–88.
[44] Kauzmann W. The nature of the glassy state and the behavior of liquids at low temperatures. Chem Rev 1948;43(2):219–56.
[45] Clavaguera-Mora MT. Glassy materials: thermodynamic and kinetic quantities. J Alloys Compd 1995;220(1):197–205.
[46] Gates SD. Cation influence on negative thermal expansion in the $A_2M_3O_{12}$ family (Doctoral dissertation). University of Toledo; 2008.
[47] Terashima K, Hashimoto T, Uchino T, Kim SH, Yoko T. Structure and nonlinear optical properties of Sb_2O_3-B_2O_3 binary glasses. Nippon Seramikkusu Kyokai Gakujutsu Ronbunshi 1996;104(11):1008–14.
[48] Som T, Karmakar B. Structure and properties of low-phonon antimony glasses and nano glass-ceramics in K_2O–B_2O_3-Sb_2O_3 system. J Non-Cryst Solids 2010;356(20):987–99.
[49] Zhenhua L. Chemical bond approach to the chalcogenide glass forming tendency. J Non-Cryst Solids 1991;127(3):298–305.
[50] Bach H, Neuroth N. The properties of optical glass. Springer Science & Business Media; 2012.
[51] Bach H, Krause D. Analysis of the composition and structure of glass and glass ceramics. Springer Science & Business Media; 2013.
[52] Mazurin OV, Porai-Koshits EA. Phase separation in glass. Elsevier; 1984.
[53] Milyukov EM, Kind NE. Phase-separation phenomena in glasses of aluminosilicate systems containing various modifier cations. In: Phase-Separation Phenomena in Glasses/Likvatsionnye Yavleniya v Steklakh/Ликвационные Явления в Стеклах. Springer, US; 1973. pp. 158–161.
[54] Ojovan MI, Lee WE. An introduction to nuclear waste immobilisation. Newnes; 2013.
[55] Muruganandam K, Seshasayee M. Structure studies on mixed glass former Li_2O–P_2O_5–Sb_2O_3 system. Phys Chem Glasses 1999;40(5):287–91.
[56] Lupton DF, Merker J, Schoélz F. The correct use of platinum in the XRF laboratorys. X-Ray Spectrom 1997;26(132):140.
[57] Altaf M, Chaudhry MA. Effect of crucible material on optical bandgap and activation energy of Na_2O-CdO-P_2O_5 glasses. J Mater Sci 2005;40(15):4019–23.
[58] de La Parra-Arciniega SM, Álvarez-Méndez A, Torres-González LC, Sánchez EM. Crystallization kinetics of a soda lime silica glass with TiO_2 addition. Revista Mexicana De física 2009;55(1):32.
[59] His CS, Wang MC. Crystallization kinetics and phase transformation of Li_2O-Fe_2O_3-MnO_2-CaO-P_2O_5-SiO_2 glass. J Mater Res 1998;13(09):2655–61.
[60] El-Meliegy E, van Noort R. Glasses and glass ceramics for medical applications. Springer Science & Business Media; 2011.
[61] Taibi Y, Poulain M, Lebullenger R, Atoui L, Legouera M. Physical properties of new Sb_2O_3-V_2O_5-K_2O glasses; 2014.
[62] Gabbott P. Principles and applications of thermal analysis. John Wiley & Sons; 2008.
[63] Niida Haruki, Takahashi Masahide, Uchino Takashi, Yoko Toshinobu. Preparation and structure of organic–inorganic hybrid precursors for new type low-melting glasses. J Non-Cryst Solids 2002;306(3):292–9.
[64] Kosuge T, Benino Y, Dimitrov V, Sato R, Komatsu T. Thermal stability and heat capacity changes at the glass transition in K_2O-WO_3-TeO_2 glasses. J Non-Cryst Solids 1998;242(2):154–64.
[65] Wagh A, Ajithkumar MP, Kamath SD. Composition dependent structural and thermal properties of Sm_2O_3 doped zinc fluoroborate glasses. Energy Res J 2014;4(2):52–8.
[66] Iskandar SM, Halimah MK, Daud WM, Sidek HAA, Zaman K. Thermal stability and physical properties of PbO-B_2O_3-TeO_2 glass system. Solid State Sci Technol 2012;20(1 & 2):48–55.
[67] Sahar MR, Sazali ES. Physical and thermal properties of TeO_2-Na_2O-MgO doped Eu_2O_3 Glass; 2010.
[68] Lee ETY, Taylor ERM. Compositional effects on the optical and thermal properties of potassium aluminophosphate glasses. Opt Mater 2004;27(2):323–30.
[69] Aboutaleb D, Safi B, Ayadi A, Iratni A. Effect of the AL_2O_3 and BaO addition on the thermal and physical properties of ternary glass system (B_2O_3-BaO-AL_2O_3); 2013.
[70] Aboutaleb D, Safi B. Lithium oxide effect on the thermal and physical properties of the ternary system glasses (Li_2O_3-B_2O_3-Al_2O_3). Int J Chem Mol Nucl Mater Metall Eng 2015;9(3):425–8.
[71] Cleek GW, Babcock CL. Properties of Glasses in some ternary systems containing BaO and SiO_2. The University of Arizona Tucson Optical Science Center; 1973.
[72] Khanna A, Saini A, Chen B, González F, Ortiz B. Structural characterization of PbO-B_2O_3-SiO_2 glasses. Phys Chem Glasses Eur J Glass Sci Technol Part B 2014;55(2):65–73.
[73] Mocioiu OC, Zaharescu M, Atkinson I, Mocioiu AM, Budrugeac P. Study of crystallization process of soda lead silicate glasses by thermal and spectroscopic methods. J Therm Anal Calorim 2014;117(1):131–9.
[74] Franks K, Abrahams I, Georgiou G, Knowles JC. Investigation of thermal parameters and crytallisation in a ternary CaO-Na_2O-P_2O_5-based glass system. Biomaterials 2001;22(5):497–501.
[75] Schwarz J, Vosejpkova K. Thermal properties of Ga_2O_3-PbO-P_2O_5 glass system. J Therm Anal Calorim 2011;104:1051–4.
[76] Narayanan MK, Shashikala HD. Thermal and optical properties of BaO-CaF_2-P_2O_5 glasses. J Non-Cryst Solids 2015;422:6–11.
[77] Allen JP, Carey JJ, Walsh A, Scanlon DO, Watson GW. Electronic structures of antimony oxides. J Phys Chem C 2013;117(28):14759–69.
[78] Satyanarayana T, Kityk IV, Ozga K, Piasecki M, Bragiel P, Brik MG, Veeraiah N. Role of titanium valence states in optical and electronic features of PbO–Sb_2O_3–B_2O_3:TiO_2 glass alloys. J Alloys Compd 2009;482(1):283–97.
[79] Steinkemper H, Fischer S, Hermle M, Goldschmidt JC. Stark level analysis of the spectral line shape of electronic transitions in rare earth ions embedded in host crystals. New J Phys 2013;15(5):053033.
[80] Huang YD, Mortier M, Auzel F. Stark levels analysis for Er^{3+}-doped oxide glasses: germanate and silicate. Opt Mater 2001;15(4):243–60.
[81] Huang YD, Mortier M, Auzel F. Stark level analysis for Er^{3+}-doped ZBLAN glass. Opt Mater 2001;17(4):501–11.